Band Structure and Optical Absorption in Multilayer Armchair Graphene Nanoribbons: A Pariser-Parr-Pople Model Study

Kondayya Gundra[1, *] and Alok Shukla[1]

[1]*Department of Physics, Indian Institute of Technology, Bombay, Mumbai 400076 INDIA*

Using the tight binding and Pariser-Parr-Pople (PPP) model Hamiltonians, we study the electronic structure and optical response of multilayer armchair graphene nanoribbons (AGNRs), both with and without a gate bias. In particular, the influence of the number of layers (n), and the strength of the electric field applied perpendicular to layers, for different types of edge alignments, is explored on their electro-optical properties. As a function of increasing n, the energy gap initially decreases, eventually saturating for large n. The intensity of the linear optical absorption in these systems also increases with increasing n, and depends crucially on the polarization direction of the incident light, and the type of the edge alignment. This provides an efficient way of determining the nature of the edge alignment, and n, in the experiments. In the presence of a gate bias, the intensity of optical absorption behaves in a nontrivial way. The absorption becomes more intense for the large fields in narrow ribbons exhibiting a red shift of the band gap with the increasing field strength, while in broad ribbons exhibiting a blue shift, the absorption becomes weaker. However, for smaller electric fields, the absorption intensity exhibits more complicated behavior with respect to the field strength. Thus, the effect of the gate bias on optical absorption intensity in multilayer AGNRs is in sharp contrast to the bilayer graphene, which exhibits only enhancement of the absorption intensity with the increasing electric field.

I.   INTRODUCTION

Since the isolation of graphene[1], rapid advances have been made in the experimental[2] and theoretical[3–5] investigations of this truly two dimensional (2D) material, and related nanostructures, for use in the next generation opto-electronic devices.[6,7] While graphene is a zero gap semiconductor, energy gap opens up in quasi one-dimensional (1D) graphene nanoribbons (GNRs) due to reduced dimensions. The mechanism of gap opening in GNRs depends on the nature of the edge termination. First principles calculations[8,9] show that, in case of mono-layer zigzag GNRs (ZGNRs) energy gaps open up due to edge magnetism. On the other hand, the gap opening in mono-layer armchair GNRs (AGNRs), is believed to be both due to quantum confinement, and the reduction of the bond lengths at the edges.[8]

While numerous theoretical studies of the electronic structure and related properties of the mono-layer GNRs exist,[10] relatively fewer calculations on bilayer and multilayer-GNRs have been performed.[11–20] Recently, gated bilayer graphene has attracted a great deal of attention in the experimental,[21–25] as well as theoretical communities.[26–30] The energy gap in bilayer graphene, in the presence of a transverse electric field, has been found to be tunable over a wide range of values (up to 250 meV).[21,23] Furthermore, the electrical noise levels in bilayer graphene channels is much less compared to the noise levels in single layer graphene,[22] thus making bilayer graphene, a promising candidate for the fabrication of high-quality electronic devices. Based upon this, one can argue that compared to mono-layer GNRs, bilayer GNRs will possess superior properties from the point of view of device physics. Moreover, it is interesting to study multilayer graphene and GNRs in their own right, as they can help us in understanding the evolution of the electronic structure from graphene to bulk graphite.[31]

Recently, we have developed an approach to study the electronic structure of graphene nanostructures, based upon the π-electron Pariser-Parr-Pople (PPP) model Hamiltonian,[32] and used it to study the band structure, edge magnetism, and optical absorption of mono-layer GNRs of various types, at the Hartree-Fock level.[33] The advantage of the PPP model based methodology is that it incorporates the long-range Coulomb interactions among the π-electrons in a natural way. In this work, we apply our approach[33] to perform a detailed investigation of the electronic structure of multilayer AGNRs, with and without an external electric field, and for various edge alignments. For the gated ribbons with the intrinsic band gaps above a critical value (say, ϵ_c), the gap decreases with the increasing field strength, while for those with gaps lower than ϵ_c, it increases with the external field, a result in good agreement with the recent *ab initio* results of Sahu *et al.*[20] In addition to the studies of the band structure, we also present calculations of the optical absorption spectra of various multilayer AGNRs for different edge alignments, for various polarization directions of the incident light, and with, and without, a gate bias. To the best of our knowledge, no prior calculations of optical absorption in multilayer-GNRs exist, which take electron-electron interactions into account. Our calculations reveal that for the gated bilayer ribbons, for large bias fields, the optical absorption intensity increases for the ribbons with the intrinsic band gaps higher than ϵ_c, while for the ribbons with the gaps smaller than ϵ_c, the

absorption intensity decreases. However, for smaller bias fields, the absorption intensity exhibits a more complicated behavior with respect to the field strength, a behavior in sharp contrast with the gated bilayer graphene which exhibits only increase in the absorption intensity with the increasing bias field.[21,23,30] Furthermore, we find that in addition to the polarization direction, the absorption intensity is found to be crucially dependent on the number of layers in the multilayer AGNRs, and their edge alignment, thereby allowing for optical determination of their structure.

The remainder of this paper is organized as follows. In section II, we briefly describe our PPP model based theoretical methodology. Next, in Sec. III we present the results of our calculations on the band structure of various multilayer AGNRs, and discuss the variation of the band gap with the increasing number of layers, their widths, and as a function of the gate bias. In section IV we present the optical absorption spectra of these systems, and discuss their variation with n, external electric field, and the type of edge alignment. Finally, in Sec V we summarize our results, and present the conclusions.

II. THEORETICAL METHODOLOGY

In our earlier works we have used the PPP model to extensively to study the electronic structure and optical properties of *finite* π-electron systems such as conjugated molecules and oligomers at various levels of theory,[34] while in our recent work we extended it to study GNRs in the infinite length limit, with 1D periodic boundary conditions imposed.[33] The PPP model Hamiltonian,[32] with one π-electron per carbon atom, is given by

$$H = -\sum_{i,j,\sigma} t_{ij}(c_{i\sigma}^\dagger c_{j\sigma} + c_{j\sigma}^\dagger c_{i\sigma}) +$$

$$U \sum_i n_{i\uparrow} n_{i\downarrow} + \sum_{i<j} V_{ij}(n_i - 1)(n_j - 1) \tag{1}$$

where $c_{i\sigma}^\dagger$ creates an electron of spin σ on the p_z orbital of carbon atom i, $n_{i\sigma} = c_{i\sigma}^\dagger c_{i\sigma}$ is the number of electrons with the spin σ, and $n_i = \sum_\sigma n_{i\sigma}$ is the total number of electrons on atom i. The parameters U and V_{ij} are the on-site and long-range Coulomb interactions, respectively, while t_{ij} is the one-electron hopping matrix element. On setting $U = V_{ij} = 0$, the Hamiltonian reduces to tight binding (TB) model, while on setting just $V_{ij} = 0$, it reduces to the Hubbard model. The parametrization of Coulomb interactions is Ohno like,[35]

$$V_{i,j} = \frac{U}{\kappa_{i,j}(1 + 0.6117 R_{i,j}^2)^{1/2}} , \tag{2}$$

where, $\kappa_{i,j}$ depicts the dielectric constant of the system which can simulate the effects of screening, and $R_{i,j}$ is the distance in Å between the i-th and the j-th carbon atoms. In our earlier work on GNRs,[33] we used the *ab-initio* GW band structure of mono layer AGNR-12 (AGNR-N_A, denotes an AGNR with N_A dimer lines across the width) reported by Son *et al.*[8] to obtain a set of "modified screened Coulomb parameters," with $U = 6.0$ eV and $\kappa_{i,j} = 2.0$ ($i \neq j$) and $\kappa_{i,i} = 1$. Note that our modified screened parameters are slightly different from the screened parameters reported initially by Chandross and Mazumdar,[36] with $U = 8.0$ eV and $\kappa_{i,j} = 2.0$ ($i \neq j$) and $\kappa_{i,i} = 1$, aimed at describing the optical properties of phenyl-based polymers within the PPP model. With our modified screened parameters, we obtained excellent agreement between the *ab initio* GW band gaps,[8] and our PPP Hartree-Fock band gaps for mono layer AGNRs of various widths,[33] therefore, we have used these parameters in the present study of multilayer AGNRs as well.

In these calculations, we consider Bernal packed multilayer AGNRs with ABAB... repeat pattern, and two possible edge alignments, called α and β alignments,[13] shown in Fig. 1. The intra layer nearest-neighbor (NN) distance was taken to be 1.42 Å, and, for the inter layer separation the value 3.35 Å, identical to that in graphite, was used. As far as the hoppings are concerned, the intra layer NN hopping was chosen to be $t = 2.7$ eV, along with the next-nearest-neighbor (NNN) hopping $t' = 0.27$ eV. For the inter-layer hopping also, we considered not only NN hopping $t_\perp = 0.4$ eV, but also the NNN hopping integral $t'_\perp = 0.3$ eV.[3] We further explore the parameter dependence of the calculated optical absorption spectra in section IV B. Because multilayer AGNRs are closed-shell insulating systems, like their mono layer counterparts, we used the restricted HF (RHF) method to obtain the band structure in our calculations, as described in our previous work.[33]
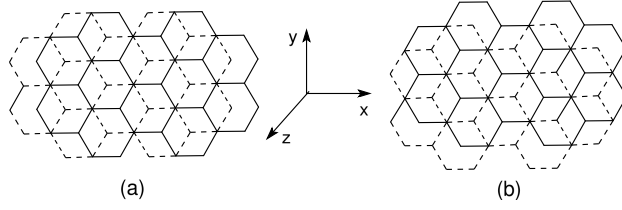
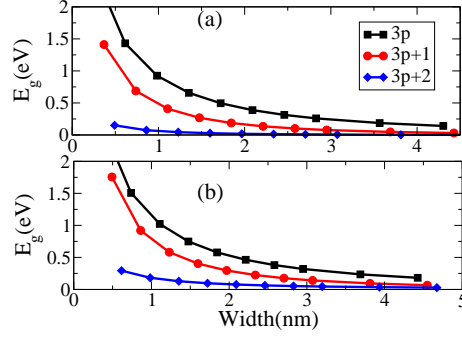Figure 1: The structures of bilayer AGNR (a) α-alignment and (b) β-alignment

Figure 2: (Color online) Variation of the energy gap with the increasing width for bilayer AGNRs, obtained by the tight-binding method for (a) α-alignment (b) β-alignment.

III.   ENERGY GAPS AND BAND STRUCTURE

A.   Energy gaps

The TB calculations on mono-layer AGNRs[37] predicted that AGNR$-N_A$ with $N_A = 3p$ and $N_A = 3p + 1$ (p is a positive integer) exhibit energy gaps ($E_g^{N_A}$), which are inversely proportional to N_A, whereas AGNRs with $N_A = 3p + 2$ are gapless. Hence, based upon TB theory, they can be classified into three groups with energy gaps varying as $E_g^{3p} \geq E_g^{3p+1} \geq E_g^{3p+2}(= 0)$. However, *ab initio* density-functional theory (DFT) calculations[8] on these ribbons predicted a different relationship $E_g^{3p+1} \geq E_g^{3p} \geq E_g^{3p+2}(\neq 0)$, with the important result that even for $N_A = 3p + 2$, AGNRs exhibit nonzero energy gaps, due to the fact that the bond lengths involving the edge atoms are shorter than those in the interior. When the decrease in the bond length is incorporated in the TB approach by increasing the corresponding hopping, one also obtains finite gaps for $N_A = 3p + 2$ ribbons, although the relation $E_g^{3p} \geq E_g^{3p+1} \geq E_g^{3p+2}$ still holds. Based upon first principles DFT calculations Sahu *et al.*,[13,20] discovered that for bilayer AGNRs, and other multilayer AGNRs $E_g^{3p+1} \geq E_g^{3p} \geq E_g^{3p+2}(\neq 0)$ is valid, in full agreement with the DFT results of Son *et al.*[8] obtained for the mono-layer AGNRs. In what follows we first explore the same relationship using the TB model, and in Figs. 2 and 3 we present the variation of the energy gaps of different families of bilayer and eight layer AGNRs, respectively, with respect to their widths, both for the α and the β alignments. The values of of the hopping integrals used in these calculations were as specified in section II, except that the hoppings at the edges were increased by 12%,[8] leading to finite band gaps for ribbons with $N_A = 3p + 2$ for the narrow multilayer ribbons. As is obvious from the figure, our results are consistent with the aforesaid relation $E_g^{3p} \geq E_g^{3p+1} \geq E_g^{3p+2}$ valid for mono-layer AGNRs at the TB level. Furthermore, for a given width of the bilayer and eight layer AGNRs, band gaps with the β alignment are always more than that for the α alignment.

Next, for each of the three families of AGNRs, we examine the variation of the gap as a function of the increasing number of layers (n) at the TB level, and results of our calculations are presented in Fig. 4a for the α alignment, and in Fig. 4b for the β alignment. Although, these calculations were performed for $p = 3$, a similar behavior was also observed for other values of p. We find that: (a) again the band gaps for the ribbons in β-alignment are larger than those for the α-alignment, and (b) band gaps for both types of alignments saturate fairly rapidly with respect to n, suggesting that a small number of layers are needed to achieve the bulk values.

In particular, for the α-aligned ribbons with $N_A = 11$ ($3p + 2$ class) , the band gap decreases rapidly with n and becomes negligibly small for large values of n (Fig.4(a), blue/dashed line) whereas, for the β alignment the band gap is much less sensitive to n and attains a constant value, for smaller values of n (Fig.4(b), blue/dashed line). This
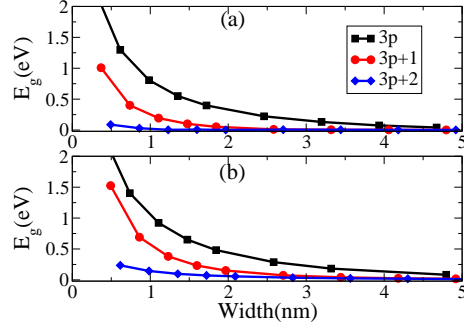
Figure 3: (Color online) Variation of the energy gap with the increasing width for the AGNRs with eight layers, obtained by the tight-binding method for (a) α-alignment (b) β-alignment.
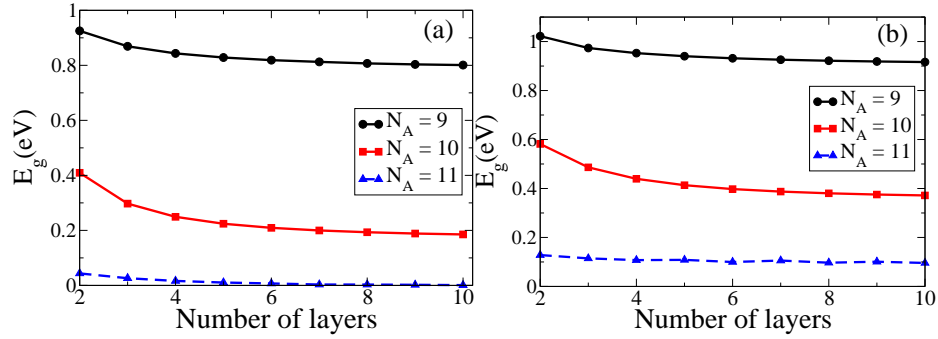

Figure 4: (Color online) Variation of energy gap with number of layers obtained by the tight-binding method for multilayer AGNRs in (a) α-alignment (b) β-alignment.

tendency holds even when the e-e interactions are considered, as is evident in the Fig. 5 which presents the variation of band gap with number of layers for multilayer AGNRs with $N_A = 8$ in α-alignment (black line) and in β-alignment (red line), obtained by PPP-RHF approach. From the results it is obvious that the inclusion of the e-e interactions leads to the widening up of the band gaps, compared to the TB approach.

B.   Band structure

For the sake of brevity, in what follows, we denote a given multilayer AGNR as n-AGNR-N_A-α (n-AGNR-N_A-β), implying an AGNR with n layers, each of width N_A, arranged in α (β) alignment. In our previous work we have emphasized the role of long-range e-e interactions in widening the band gaps of the mono-layer AGNRs.[33] For example,
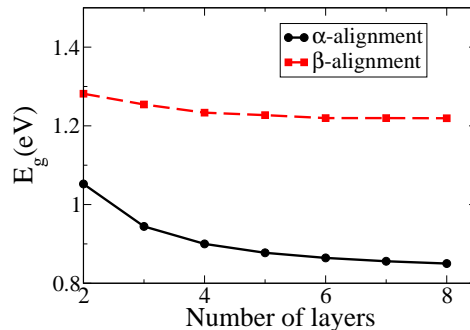

Figure 5: (Color online) Variation of energy gap with number of layers obtained using the PPP model, within the RHF approximation, for the multilayer AGNRs with $N_A = 8$, in α and β alignments.
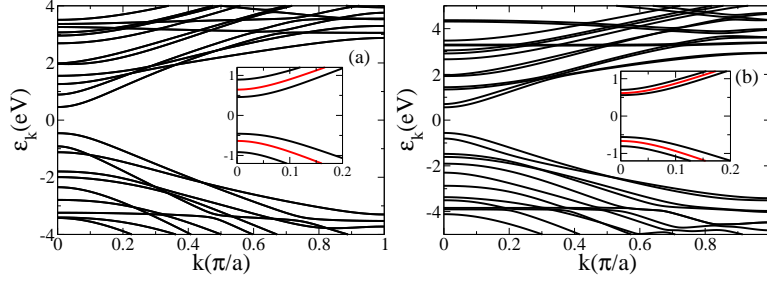
Figure 6: (Color online) Band structure of (a) 2-AGNR-11-α , (b) 2-AGNR-11-β, obtained using the PPP-RHF approach. The inset contains the magnified band structure near the Fermi energy ($E_F = 0$) of: (a) 2-AGNR-11 (black lines) and (b) mono-layer AGNR-11 (red lines).

we demonstrated that for mono-layer AGNR-11, the Hubbard model based calculations predict a negligible gap, while the PPP-RHF method predicts a gapped system in agreement with the GW calculations.[8] We expect the long-range e-e interactions, as incorporated in the PPP model, to play a similar role for multilayer AGNRs as well. According to the *ab initio* DFT calculations of Sahu *et al.*[13,20], all n-AGNR-N_A-α, of the family $N_A = 3p+2$, exhibit much smaller gaps compared to the other families, suggesting a metal-like behavior. In Figs. 6a and 7 we present the PPP-RHF band structures of a few members of this family, 2-AGNR-11-α, 3-AGNR-8-α, 4-AGNR-8-α, and 10-AGNR-8-α, and from the figures it is obvious that all these ribbons have substantial band gaps. Therefore, we believe that the *ab initio* results of Sahu *et al.*[13,20] reporting these systems as almost metallic, are due to the well-known tendency of the DFT to underestimate the gaps, and that a better estimate of the gap can only be made by some electron-correlated approach such as the GW approximation.[8]

We investigate the effect of edge alignment on the band structure of bilayer AGNRs by presenting the band structure of 2-AGNR-11-α (Fig.6 (a)), and 2-AGNR-11-β (Fig.6(b)). The band structure near the Fermi energy is magnified in the insets of those figures, which also contain the band structure of mono-layer AGNR-11. In the presence of the second layer, each mono-layer band is split into two bands: one with the lower energy and the other with the higher energy, thus reducing the gap. From insets of Figs. 6a and 6b, it is clear that the valence and the conduction bands formed due to the aforesaid band splitting for 2-AGNR-11-α near E_F are separated by larger energy compared to the case of 2-AGNR-11-β. Therefore, it suggests that the perturbation introduced by the second layer is larger in the case of the α-aligned AGNRs, as compared to the β-aligned AGNRs, for which we offer the following geometrical explanation. Intuitively speaking, the layers will interact with each other the most if they were stacked in the AA arrangement (with all the carbon atoms on top of each other), leading to a more prominent band splitting, and thus the smallest gap possible from various stacking arrangements. For the AB stacking, however, in the α case, the difference with respect to the AA stacking is much less because the layers are only displaced in the x direction, while in the β case, layers are displaced both in the x as well as the y directions, resulting in more disalignment compared to the α case (*cf*. Fig. 1). Therefore, in α alignment the layers will interact with each other more than those in the β case, resulting in a band structure more distinct compared to a mono-layer, and, thus, a smaller gap, compared to the β case. We verified this hypothesis by actually performing the band structure calculations for 2-AGNR-11 in different stacking patterns and alignments, and the band gaps (in eV) obtained by using the TB/PPP-RHF method were 0.02/0.43 (AA), 0.04/0.92 (AB-α) and 0.13/1.12 (AB-β).

Next, we illustrate the variation in the band structure with the number of layers (n), by presenting the band structure near E_F of 3-AGNR-8-α (Fig.7a), 4-AGNR-8-α (Fig.7b), and 10-AGNR-8-α (Fig.7c). The band structure changes significantly with increasing n, leading not just to more bands, but also causing bands near E_F to become flatter. Furthermore, this flatness extends more and more into BZ as n increases, which shows up as a tremendous increase in the joint density of states not just due to a denser band structure, but also due to van Hove singularity like increase caused by parallel bands. This has obvious implications for the optical absorption spectra of such ribbons, which will be discussed further in Sec. IV D.

C. Effect of gate bias on the electronic structure

The variation of band gaps of bilayer AGNRs, when electric (E_z) is applied along z-direction is quite interesting. *Ab initio* DFT study on these systems by Sahu *et al.*,[13] revealed that the band gaps increase with the increasing E_z for ribbons with band gaps below a critical value, and decrease for ribbons with band gaps above this critical value. Using nearest neighbor TB approach, coupled with perturbation theory, they showed that for the α-aligned ribbons,
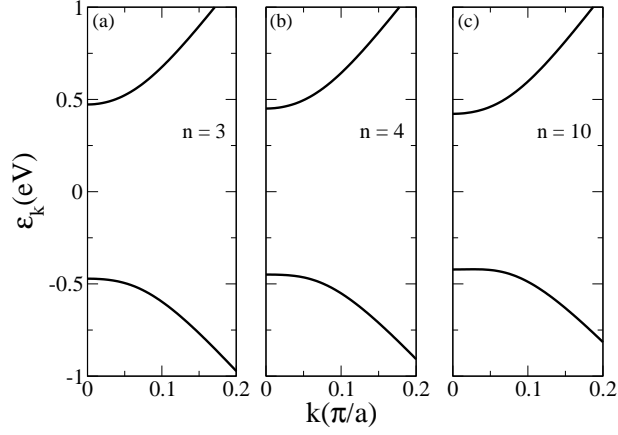
Figure 7: Band structure of (a) 3-AGNR-8-α , (b) 4-AGNR-8-α, (c) 10-AGNR-8-α near E_F obtained using the PPP-RHF approach.
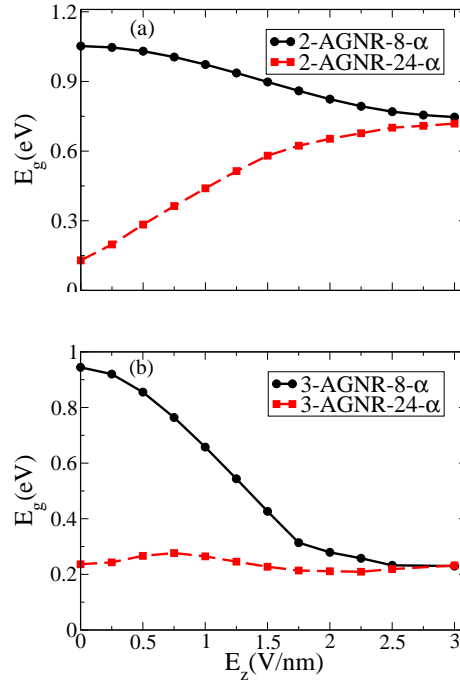

Figure 8: (Color online) Variation of energy gap with E_z for (a) 2-AGNR-8-α and 2-AGNR-24-α (b) 3-AGNR-8-α and 3-AGNR-24-α, obtained using the PPP-RHF approach.

the critical band gap $\epsilon_c = (\sqrt{5} - 1)t_\perp$, so that for $t_\perp = 0.4$, i $\epsilon_c \approx 0.25$ eV. In Fig. 8a we present the variation of band for 2-AGNR-8-α and 2-AGNR-24-α with E_z, obtained using the PPP-RHF calculations. In the absence of E_z, the band gap of 2-AGNR-8-α is larger than the ϵ_c, hence the band gap decreases with E_z (Fig. 8a, black solid line), whereas, the band gap of 2-AGNR-24-α in the absence of E_z is less than ϵ_c, hence the band gap increases with E_z (Fig. 8a, red lines). In Fig. 8b we present the variation of band gap for 3-AGNR-8-α and 3-AGNR-24-α with E_z, and we observe a trend similar to the case of the bilayer GNRs for 3-AGNR-8-α, but for 3-AGNR-24-α the gap exhibits small oscillations around a uniform value. The trends on the variation of band gaps with E_z, obtained from our PPP-RHF calculations are fully consistent with the *ab initio* DFT results.[13,20]

Finally, we examine the variations in the band structures of multilayer AGNRs caused by the gate bias. In the absence of an external electric field, the fundamental gap of all the ribbons is located at $k = 0$. However, when the electric filed is applied, location of the fundamental gap shifts in the BZ, from $k = 0$ to finite values of k, similar to what was observed in the gated multi-layer graphene as well.[38] The rightward shift of fundamental gap continues with the increasing E_z which is evident from the Fig. 9 , where we have presented the band structure of of 3-AGNR-24-α
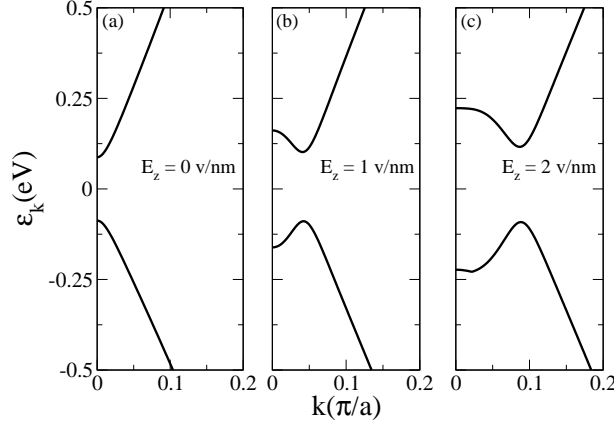
Figure 9: PPP-RHF band structure of 3-AGNR-24-α near E_F, for several values of external electric field E_z

for increasing values of E_z.

IV. OPTICAL ABSORPTION SPECTRA

A. Basic formalism

The optical absorption spectrum for incident radiation polarized in x or y or z direction is computed in the form of the corresponding components of the imaginary part of the dielectric constant tensor, $i.e.$, $\epsilon_{ii}(\omega)$ using the standard formula

$$\epsilon_{ii}(\omega) = C \sum_{v,c} \int_{-\pi/a}^{\pi/a} \frac{|\langle c(k)|p_i|v(k)\rangle|^2}{\{(E_{cv}(k) - \hbar\omega)^2 + \gamma^2\}E_{cv}^2(k)} dk, \tag{3}$$

where a is the 1D lattice constant, $|c(k)\rangle$ ($|v(k)\rangle$) denotes conduction (valence) band state, p_i denotes the momentum operator in the i-th Cartesian direction, ω represents the angular frequency of the incident radiation, $E_{cv}(k) = \epsilon_c(k) - \epsilon_v(k)$, with $\epsilon_c(k)$ ($\epsilon_v(k)$) being the conduction (valence) band eigenvalues of the Fock matrix, γ is the line width, while C includes rest of the constants. As in our previous work,[33] the momentum matrix elements $\langle c(k)|p_i|v(k)\rangle$ were computed numerically using the formula proposed by Pedersen $et\ al.$[39]

B. Sensitivity of the optical absorption to Hamiltonian parameters

Before we present and discuss our results on the optical absorption in multilayer ANGRs, we examine their sensitivity to the hopping and the Coulomb parameters used in the PPP model Hamiltonian. We used two sets of Coulomb parameters: $U = 6.0$ eV and $\kappa_{i,j} = 2.0$ ($i \neq j$) and $\kappa_{i,i} = 1$ (our modified screened parameters[33]) and $U = 8.0$ eV and $\kappa_{i,j} = 2.0$ ($i \neq j$) and $\kappa_{i,i} = 1$ (original screened parameters of Chandross and Mazumdar[36]). Similarly, for the hoppings we used two sets: commonly used values of $t = 2.7$ eV ,$t^{'} = 0.27$ eV, $t_{\perp} = 0.4$ eV, $t_{\perp}^{'} = 0.3$ eV, and a set with larger values of hoppings, $viz.$, $t = 3.16, t^{'} = 0.316$, $t_{\perp} = 0.39$ eV, and $t_{\perp}^{'} = 0.315$.[40] In Figs. IV B and IV B we present the results of these calculations for the ribbons 2-AGNR-11-α and 2-AGNR-12-α, respectively. From the figures the following trends emerge: (a) For 2-AGNR-11-α, the change of hoppings (red line vs black line) does not change the results significantly, but the increase in the value of U ($U = 6$ vs. $U = 8$) leads to a prominent blue shift in the spectrum, (b) For 2-AGNR-12-α, however, the situation is different because change in hopping leads to more significant changes in the spectrum, as compared to the change in U. Therefore, the dependence of the optical absorption on the Hamiltonian parameters is itself dependent on the nature of the multilayer ribbon concerned. Because, at present no experimental information is available as to the optical absorption spectra of GNRs, thus, it is impossible to judge as to what are the correct set of parameters to be used in the Hamiltonian. Therefore, given our past experience with the modified screened parameters ($U = 6.0$ eV and $\kappa_{i,j} = 2.0$ ($i \neq j$) and $\kappa_{i,i} = 1$), and the
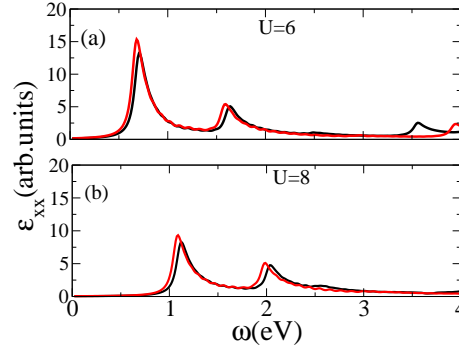
Figure 10: (Color online) Optical absorption spectra of 2-AGNR-11-α calculated using the PPP-RHF approach for the light polarized along the x axis with Coulomb parameters (a) $U = 6.0$ eV and $\kappa_{i,j} = 2.0$ ($i \neq j$) and $\kappa_{i,i} = 1$ and (b) $U = 8.0$ eV and $\kappa_{i,j} = 2.0$ ($i \neq j$) and $\kappa_{i,i} = 1$. In both the cases the black lines correspond to hopping parameters (in eV) $t = 2.7$, $t' = 0.27$, $t_\perp = 0.4$ eV, and $t'_\perp = 0.3$, the red line corresponds to $t = 3.16$, $t' = 0.316$, $t_\perp = 0.39$ eV, and $t'_\perp = 0.315$.
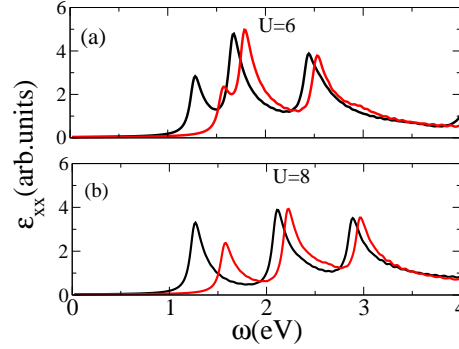

Figure 11: (Color online) Optical absorption spectra of 2-AGNR-12-α computed using the PPP-RHF approach for the light polarized along the x axis, with various sets of PPP parameters as explained in the caption of Fig. IV B.

in-plane hopping $t = 2.7$ eV for the mono-layer GNRs,[33] in the remainder of this work we utilize modified screened parameters and the hopping values $t = 2.7$ eV ,$t' = 0.27$ eV, $t_\perp = 0.4$ eV, $t'_\perp = 0.3$ eV.

C. Effect of edge alignment on the absorption spectrum

In order to investigate the sensitivity of optical absorption to the type of edge alignment, we present the optical absorption spectra of 2-AGNR-8 in α and β alignments. In Fig. 12 a we present the optical absorption spectrum for light polarized along the periodicity direction (x axis, $\epsilon_{xx}(\omega)$), where Σ_{mn} denotes a peak in the spectrum due to a transition from m-th valence band (counted from the top) to the n-th conduction band (counted from the bottom). For α-alignment (black line), the first peak of $\epsilon_{xx}(\omega)$ at 1.06 eV is Σ_{11}, while the one at 1.96 eV represents Σ_{22}. For the β alignment (red line) Σ_{11} peak is located at 1.30 eV, while the second peak (Σ_{22}) at 1.67 eV. The separation between the first two peaks is larger in the case of α-alignment, as compared to that in the β alignment. This is a consequence of the observation discussed in Sec. III B that the energy separation between the adjacent bands near Fermi energy at $k = 0$ is larger in the α-alignment compared to β -alignment.

In Fig. 12b, the absorption spectra corresponding to the y-polarized photons ($\epsilon_{yy}(\omega)$) is presented, and the first peak for the α alignment (black line) located at 2.61 eV represents Σ_{14}, the second peak at 2.69 eV is Σ_{22}, while the peak at 3.3 eV is Σ_{51}. Significant differences in $\epsilon_{yy}(\omega)$ are observed for the β alignment: it starts with two tiny peaks, with the first one (Σ_{11}) at 1.30 eV, and the second one at 1.67 eV (Σ_{22}), which were absent in case of the α alignment. The intense peaks for β -alignment are located at 2.62 eV (Σ^{14}), which is coincidental with the same peak for the α case, and 3 eV ($\Sigma_{41}+\Sigma_{23}$) which is located in the similar energy range as the higher peaks of the α case.

Finally, we examine the z polarized component of the absorption spectra ($\epsilon_{zz}(\omega)$) presented in Fig. 12c, for 2-AGNR-8. In the low energy regime $\epsilon_{zz}(\omega)$ follows $\epsilon_{xx}(\omega)$ very closely , but the magnitude of the peaks of $\epsilon_{zz}(\omega)$ is reduced significantly compared to the peaks of $\epsilon_{xx}(\omega)$, because of the weak inter-layer coupling. For α-alignment, the
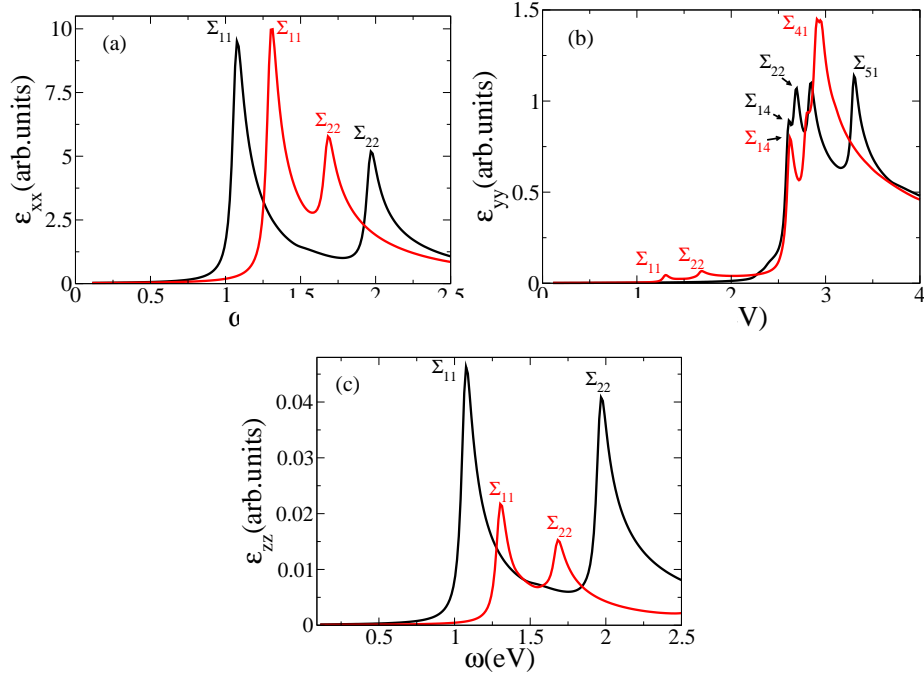
Figure 12: (Color online) Optical absorption spectra of 2-AGNR-8 calculated using the PPP-RHF approach for the light polarized along: (a) x axis (b) y axis and (c) z axis. The black lines represent the α alignment case, while the red lines denote the β alignment. A line width of 0.05 eV was assumed throughout.

peak at 1.06 eV is Σ^{11} and second peak at 1.96 eV is Σ^{22}, while for the β alignment, the corresponding peaks are at 1.30 eV, and 1.67, respectively. One very important difference in the spectra of the two types of alignments is that the peak intensities in the lower energy region are much higher in the α-alignment, than in the β-alignment.

Therefore, the absorption spectra for each polarization direction bring out distinct features depending on the type of edge alignment, which can be used in the experiments on oriented samples to determine the type of alignment.

D.   Variation of optical absorption with the number of layers

Recently, Wright *et al.*[14] using the TB calculations performed on $3p + 2$ family of bilayer AGNRs, showed that the inter-layer coupling causes strong inter subband transitions, leading to tremendous enhancement in the optical conductivity in the low-energy region, thus, making them suitable candidates for opto-electronic applications. In Fig. 13 we present the optical absorption spectra for 1-AGNR-11, 2-AGNR-11-α, and 3-AGNR-11-α, calculated using the PPP-RHF approach for the x-polarized light, with the aim of understanding the influence of n on the optical absorption. In 1-AGNR-11, the Σ^{11} peak of $\epsilon_{xx}(\omega)$ is located at 1.31 eV, while in 2-AGNR-11, and 3-AGNR-11 it becomes more intense, and successively gets red shifted to 0.94 eV and 0.84 eV, respectively. A similar trend is observed also for other transition peaks as well, as well as for the peaks in $\epsilon_{yy}(\omega)$ and $\epsilon_{zz}(\omega)$ (figures not shown). Although, the band gaps obtained using the PPP-RHF approach are much larger than that using the TB method, yet the tendency towards the enhancement of the optical response with the increasing value of n in the lower energy region is obvious from these plots. This behavior is fully consistent with the earlier discussion in Sec. III A that the enhancement of the optical response in the lower energy region of multilayer AGNRs can be understood in terms of the redshift of the fundamental gap, and the increase in the joint density of states near E_F, with increasing n.

E.   Effect of gate bias on the optical absorption

As discussed in Sec. III B, a gate bias has profound effects on the electronic structure of multilayer AGNRs, and, therefore, it is of great interest to understand the effect of electric field on the optical properties of these systems. In the Fig.14 a and 14 b we present the absorption spectrum for the x-polarized light ($\epsilon_{xx}(\omega)$) for 2-AGNR-12-α and the 2-AGNR-24-α respectively, for different values of E_z. Upon increasing the value of E_z, we observe the following trends
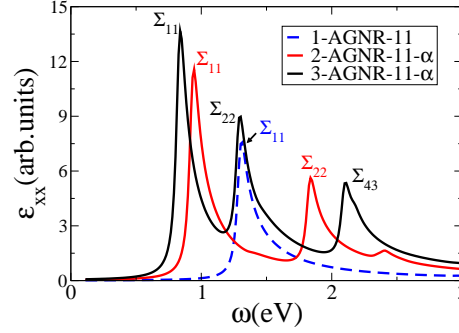
Figure 13: (Color online) Optical absorption spectra of 1-AGNR-11-α, 2-AGNR-11-α and 3-AGNR-11-α calculated using the PPP-RHF approach, for the light polarized along the x axis. A line width of 0.05 eV was assumed throughout.
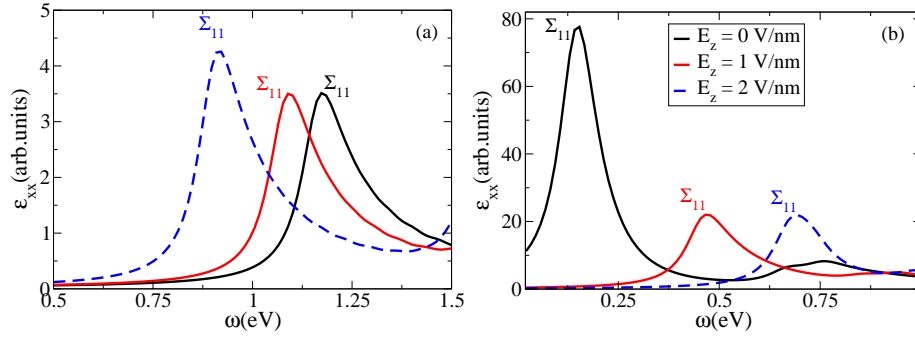

Figure 14: (Color online)PPP-RHF absorption spectra at several values of the static electric field E_z, for the incident light polarized along the x axis for (a) 2-AGNR-12-α, (b) 2-AGNR-24-α. A line width of 0.05 eV assumed throughout.

in the plot. In 2-AGNR-12-α, peak Σ_{11}, which corresponds to the fundamental gap, gets red shifted, without much change in the intensity at $E_z = 1V/nm$. But, for $E_z = 2$ V/nm, besides exhibiting the redshift, the peak also becomes more intense. In case of 2-AGNR-24-α, whose gap is less than ϵ_c, the Σ_{11} peak expectedly blue shifts with increasing E_z, however, it loses significant intensity as the field is increased from $E_z = 0$ to $E_z = 1$ V/nm. However, upon further increasing the field to $E_z = 2$ V/nm, no significant change in the intensity is observed. Thus, as far as the intensity of Σ_{11} peak with increasing gate bias is concerned, 2-AGNR-12-α and 2-AGNR-24-α behave quite differently. To elucidate this point further, in Fig.15 we present the variation of the heights of the the Σ_{11} peaks of 2-AGNR-12-α and 2-AGNR-24-α, as functions of the gate field, in the range $0 \leq E_z \leq 2.5$ V/nm. Recalling that the height of a peak is proportional to the oscillator strength of the corresponding transition, we observe the following trends: (a) for 2-AGNR-12-α the intensity varies slowly for $0 \leq E_z \leq 1.0$ V/nm, thereafter it increases monotonically, while (b) for 2-AGNR-24-α the intensity decreases rapidly for $0 \leq E_z \leq 1.0$ V/nm, and, thereafter it exhibits slow oscillations around a constant value. Thus, the two ribbons exhibit opposite behavior as far as the dependence of the oscillator strength of Σ_{11} peak on the bias field is concerned. This behavior is in sharp contrast to the experimental[21,23] and theoretical[30] results on bilayer graphene, which report a monotonic increase in the intensity of the first peak, with an increasing gate bias. This peculiar behavior of the peak intensity as a function of the gate bias can be tested in oriented samples of multilayer AGNRs, and can be used to distinguish between the widths of such ribbons.

V. SUMMARY AND OUTLOOK

In summary, we have used the PPP model based π-electron approach, incorporating long-range Coulomb interactions, to study the electronic structure and optical properties of multilayer AGNRs, at the mean-field Hartree Fock level. We considered two types of edge alignments namely α and β, both in Bernal (AB) stacking pattern, and systematically studied the variation of band gaps and optical absorption spectra of multilayer AGNRs with the increasing number of layers. These calculations have demonstrated anisotropic optical response of multilayer AGNRs, with the calculated absorption spectra being crucially dependent on the polarization direction of the incident light.
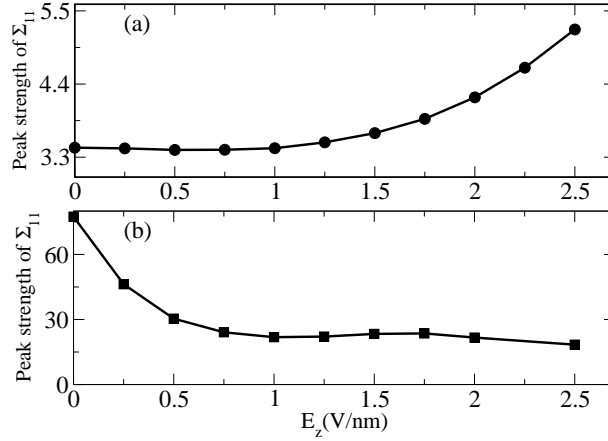
Figure 15: Variation of peak strength of Σ_{11} transition of ϵ_{xx} with static electric field E_z, computed using the PPP-RHF method, for: (a) 2-AGNR-12-α (b) 2-AGNR-24-α.

Furthermore, the optical response has been shown to depend upon the type of the edge alignment (α vs. β) and the number of layers, leading to the possible experimental determination of the nature of the edge alignment, and the number of layers in the system, using optical probes. Our calculations also reveal that a gate bias along the inter-layer direction not only alters the peak positions in the absorption spectra due to the change in the band gaps, but also the peak intensities (oscillator strengths) in a nontrivial way. The variation of the peak intensities as a function of the gate bias is of the opposite nature for the narrow and the broad bilayer AGNRs, a behavior in sharp contrast to bilayer graphene. These predictions of ours can be tested in optical experiments performed on the oriented samples of multilayer AGNRs.

As far as the future studies on multilayer AGNRs are concerned, it will be interesting to probe the influence of electron-correlation effects on various properties studied here. Furthermore, the nature of excitons in multilayer AGNRs should be investigated, so as to provide a complete description of the linear optical absorption spectra of multilayer AGNRs. Calculations along those directions are underway in our group, and results will be reported in future publications.

Acknowledgments

* Permanent Address: Theoretical Physics Division, Bhabha Atomic Research Centre, Mumbai 400085, INDIA; Electronic address: naiduk@barc.gov.in, shukla@iitb.ac.in

[1] K. S. Novoselov, A. K. Geim, S. V. Morozov, D. Jiang, Y. Zhang, S. V. Dubonos, I. V. Grigorieva, and A. A. Firsov, Science **306**, 666 (2004).

[2] M. Y. Han, B. Özyilmaz, Y. Zhang, and P. Kim, Phys. Rev. Lett. **98**, 206805 (2007); Z. Chen, Y.-M. Lin, M. J. Rooks, and P. Avouris, Physica E **40**, 228 (2007); K. A. Ritter and J. W. Lyding, Nat. Mat. **8**, 235 (2009); J. Cai, P. Ruffieux, R. Jaafar, M. Bieri, T. Braun, S. Blankenburg, M. Muoth, A. P. Seitsonen, M. Saleh, X. Feng, K. Müllen, and R. Fasel, Nature **466**, 470 (2010).

[3] A. H. C. Neto, F. Guinea, N. M. R. Peres, K. S. Novoselov, A. K. Geim, Rev. Mod. Phys. **81**, 109 (2009).

[4] N. M. R. Peres, Rev. Mod. Phys. **82**, 2673 (2010).

[5] M. Ezawa, Phys. Rev. B **73**, 045432 (2006). L. Yang, C. H Park, Y. W Son, M. L. Cohen and S. G. Louie Phys. Rev. Lett. **99**, 186801 (2007).

[6] M. Sprinkle, M. Ruan, Y. Hu, J. Hankinson, M. R. Roy, B. Zhang, X. Wu, C. Berger and W. A. de Heer, Nature Nanotechnology **5**, 727 (2010).

[7] L. Liao, Y. C Lin, M. Bao, R. Cheng, J. Bai, Y. Liu, Y. Qu, K. L. Wang, Y. Huang and X. Duan, Nature. Lett **467**, 305 (2010).

[8] Y. W. Son, M. L. Cohen, and S. G. Louie, Phys. Rev. Lett. **97,** 216803 (2006).

[9] Q. Yan, B. Huang, J. Yu, F. Zheng, J. Zang, J. Wu, B. L Gu, F. Liu, and W. Duan, Nano Lett. **7**, 1469 (2007).

[10] J. J. Palacios , J. F. Rossier , L. Brey and H. A. Fertig, Semicond. Sci. Technology **25,** 033003 (2010).

[11] H. Lee, N. Park, Y.-W. Son, S. Han, and J. Yu, Chem. Phys. Letts. **398**, 207 (2004).

[12] H. Lee, Y.-W. Son, N. Park, S. Han, and J. Yu, Phys. Rev. B **72**, 174431 (2005).

[13] B. Sahu, H. Min, A. H. MacDonald and S. K. Banerjee, Phys. Rev B, **78**, 045404 (2008).

[14] A. R. Wright, J. C. Cao, and C. Zhang, Phys. Rev. Lett. **103**, 207401 (2009).

[15] M. P. Lima, A. Fazzio, and A. J. R. da Silva, Phys. Rev. B **79**, 153401 (2009).

[16] H. Xu, T. Heinzel, I. V. Zozoulenko, Phys. Rev. B **80**, 045308 (2009).

[17] A. Cortijo, L. Oroszlány, and H. Schomerus, Phys. Rev. B **81**, 235422 (2010).

[18] X. Li, Z. Zhang, and D. Xiao, Phys. Rev. B **81**, 195402 (2010).

[19] Z. Zhang, C. Chen, X. C. Zeng, W. Guo, Phys. Rev. B **81**, 155428 (2010).

[20] B. Sahu, H. Min, and S. K. Banerjee, Phys. Rev. B **82**, 115426 (2010).

[21] E. V. Castro, K. S. Novoselov, S. V. Morozov, N. M. R. Peres, J. M. B. Lopes dos Santos, J. Nilsson, F. Guinea, and A. H. Castro Neto, Phys. Rev. Lett. **99**, 216802 (2007).

[22] Y. M. Lin and P. Avouris, Nano Lett. **8**, 2119 (2008).

[23] Y. Zhang, T. Tang, C. Girit, Z. Hao, M. C. Martin, A. Zettl, M. F. Crommie, Y. R. Shen and F. Wang, Nature **459**, 820 (2009).

[24] L. M. Zhang, Z. Q. Li, D. N. Basov, M. M. Fogler, Z. Hao, and M. C. Martin, Phys. Rev. B **78**, 235408 (2008).

[25] Z. Q. Li, E. A. Henriksen, Z. Jiang, Z. Hao, M. C. Martin, P. Kim, H. L. Stormer, and D. N. Basov, Phys. Rev. Lett. **102**, 037403 (2009).

[26] H. Min, B. Sahu, S. K. Banerjee, and A. H. MacDonald, Phys. Rev. B **75**, 155115 (2007).

[27] E. J. Nicol and J. P. Carbotte, Phys. Rev. B **77**, 155409 (2008).

[28] P. Gava, M. Lazzeri, A. M. Saitta, and F. Mauri, Phys. Rev. B **79**, 165431 (2009).

[29] B. R. K. Nanda and S. Satpathy, Phys. Rev. B **80**, 165430 (2009).

[30] L. Yang, Phys. Rev. B **81**, 155445 (2010).

[31] B. Partoens, and F. M. Peeters, Phys. Rev. B **74**, 075404 (2006).

[32] J.A. Pople, Trans. Farad. Soc **49**, 1375 (1953); R. Pariser and R.G. Parr, J. Chem. Phys. **21**, 466 (1953).

[33] K. Gundra and A. Shukla, Phys. Rev B **83**, 075413 (2011).

[34] See, *e.g.*, P. Sony and A. Shukla, Phys. Rev. B **75**, 155208 (2007); P. Sony and A. Shukla, J. Chem. Phys. **131**, 014302 (2009); P. Sony and A. Shukla, Comp. Phys. Comm, **181,** 821 (2010), and references therein.

[35] K. Ohno, Theor. Chim. Acta **2**, 219 (1964).

[36] M. Chandross and S. Mazumdar, Phys. Rev. B **55**, 1497 (1997).

[37] K. Nakada, M. Fujita, G. Dresselhaus, and M. S. Dresselhaus, Phys. Rev B **54**, 17954 (1996).

[38] A. A. Avetisyan, B. Partoens, and F. M. Peeters, Phys. Rev. B **80**, 195401 (2009); A. A. Avetisyan, B. Partoens, and F. M. Peeters, Phys. Rev. B **81**, 115432 (2010).

[39] T. G. Pedersen, K. Pedersen, and T. B. Kriestensen, Phys. Rev. B **63**, 201101(R) (2001).

[40] See, *e.g.*, H. Xu and T. Heinzel, Phys. Rev. B **80**, 045308 (2009).